Investigation of classical radiation reaction with aligned crystals

A. Di Piazza (Corresponding author)

Max-Planck-Institut für Kernphysik, Saupfercheckweg 1, D-69117, Germany

Tobias N. Wistisen, Ulrik I. Uggerhøj

Department of Physics and Astronomy, Aarhus University, 8000 Aarhus, Denmark

Abstract

Classical radiation reaction is the effect of the electromagnetic field emitted by an accelerated electric charge on the motion of the charge itself. The self-consistent underlying classical equation of motion including radiation-reaction effects, the Landau-Lifshitz equation, has never been tested experimentally, in spite of the first theoretical treatments of radiation reaction having been developed more than a century ago. Here we show that classical radiation reaction effects, in particular those due to the near electromagnetic field, as predicted by the Landau-Lifshitz equation, can be measured using presently available facilities, in the energy emission spectrum of 10-GeV electrons crossing a 0.5-mm thick diamond crystal in the axial channeling regime. Our theoretical results demonstrate the feasibility of the suggested setup, e.g., at the CERN Secondary Beam Areas (SBA) beamlines.

1. Introduction

The Lorentz equation is one of the cornerstones of classical electrodynamics and it describes the motion of an electric charge, an electron for definiteness (charge $e < 0$ and mass m), in the presence of an external, given electromagnetic field [1]. The Lorentz equation, however, does not take into account that, as the electron is being accelerated by the external field, it emits electromagnetic radiation, which in turn alters the trajectory of the electron itself (radiation reaction (RR)). The search for the equation of motion of an electron moving in a given external electromagnetic field, including self-consistently the effects of RR, has already been pursued since the beginning of the 20th century. By starting from the Lorentz equation of an electron in the presence of an external electromagnetic field and of the electromagnetic field produced by the electron itself, the so-called Lorentz-Abraham-Dirac (LAD) equation has been derived [2, 3, 4, 1, 5, 6, 7, 8]. RR effects result in two force terms in the LAD equation, one proportional to the Liénard formula for the radiated power and accounting for the energy-momentum loss of the electron due to radiation, the "damping term", and the other one, the "Schott" term, related to the electron's near field [8] and accounting for the work done by the field emitted by the electron on the electron itself [9]. Unlike the damp-

ing term, the Schott term, being proportional to the time derivative of the acceleration of the electron, 1) renders the LAD equation a non-Newtonian, third-order time differential equation; and 2) allows for unphysical features of the LAD equation as the existence of "runaway solutions", with the electron acceleration exponentially diverging in the remote future, even if, for example, the external field identically vanishes [1, 5, 6, 7, 8, 9, 10, 11].

The origin of the inconsistencies of the LAD equation has been identified in [5]. The conclusion is that in the realm of classical electrodynamics, i.e., when quantum effects can be neglected, a "reduction of order" can be consistently carried out in the LAD equation, resulting in a second-order differential equation, known as the Landau-Lifshitz (LL) equation. Moreover, the physical solutions of the LAD equation, i.e., those which are not runaway-like, have been shown to be on the critical manifold of the LAD equation itself and are governed there exactly by the LL equation [12]. Finally, the LL equation has been also derived from quantum electrodynamics in [13].

The rapid progress of laser technology has renewed the interest in the problem of RR as the strong electromagnetic fields produced by lasers can violently accelerate the electron and consequently prime a substantial emission of electromagnetic radiation. Correspondingly, a large num-

ber of setups and schemes have been recently proposed to measure classical RR effects in electron-laser interaction [14, 15, 16, 17, 18, 19] (we refer to the review [10] for previous proposals). However, experimental challenges either in the detection of relatively small RR effects or in the availability of sufficiently strong lasers has prevented so far any experimental test of the LL equation. Moreover, since RR effects are larger for ultrarelativistic electrons, reported laser-based experimental tests of the LL equation turn out to be sensitive mainly to the damping term in the LL equation, which has the most favorable dependence on the electron Lorentz factor.

In the present Letter we adopt a different perspective and put forward a presently feasible experimental setup to measure classical RR effects on the radiation field generated in the interaction of ultrarelativistic electrons with an aligned crystal. The experiment can already be performed at, e.g., the CERN Secondary Beam Areas (SBA) beamlines. In fact, in the proposed setup 10-GeV electrons impinge into a 0.5-mm thick diamond crystal and emit a significant amount of radiation due to axial channeling [20, 21, 22, 23]. Our numerical simulations indicate that in this regime RR effects substantially alter the electromagnetic emission spectrum especially at frequencies corresponding to photon energies around 0.6 GeV. Moreover, unlike experimental proposals employing lasers, the distinct structure of the electric field of the crystal at axial channeling renders the emission spectrum especially sensitive to a term in the LL equation originating from the controversial Schott term in the LAD equation. As we will see below, this term depends in general on the spacetime derivatives of the background field. This feature makes our setup prominent also with respect to synchrotron facilities where the electron dynamics is dominated by the damping term. We also mention that at an electron energy $\varepsilon_0 = 10$ GeV and for a typical synchrotron radius $R = 1$ km, the relative electron energy loss per turn is $\Delta\varepsilon/\varepsilon_0 = 8.9 \times 10^{-5}\varepsilon_0[\text{GeV}]^3/R[\text{m}] = 8.9 \times 10^{-5}$ [24], which would induce too small effects on the emitted radiation to be measured. In addition, in order for the synchrotron to operate during many turns, the electron energy loss has to be precisely compensated preventing again any possibility of "accumulating" and measuring RR on the emitted radiation.

2. The physical model

When a high-energy electron impinges onto a single crystal along a direction of high symmetry, its motion can become transversely bound and its dynamics determined by a coherent scattering in the collective, screened field of many atoms aligned along the direction of symmetry (axial channeling) [20, 21, 22, 23]. In this regime the electron experiences an effective potential in the transverse directions (continuum potential), resulting from the average of the atomic potential along the direction of symmetry. By

indicating as $\boldsymbol{z}$ the direction corresponding to the symmetry axis of the crystal and by $\boldsymbol{\rho} = (x, y)$ the coordinates in the transverse plane, with the atomic string crossing this plane at $\boldsymbol{\rho} = \mathbf{0}$, the continuum potential $\Phi(\rho)$ depends only on the distance $\rho = |\boldsymbol{\rho}|$ and it can be approximated as [22]:

$$\Phi(\rho) = \Phi_0 \left[\ln\left(1 + \frac{1}{\varrho^2 + \eta}\right) - \ln\left(1 + \frac{1}{\varrho_c^2 + \eta}\right) \right], \quad (1)$$

where $\boldsymbol{\varrho} = \boldsymbol{\rho}/a_s$ and $\varrho_c = \rho_c/a_s$. Here, the parameters Φ_0, ρ_c, η, and a_s depend on the crystal and $\rho \leq \rho_c$. A convenient choice to investigate classical RR effects is diamond, with the $\langle 111 \rangle$ as symmetry axis and for which $\Phi_0 = 29$ V, $\rho_c = 0.765$ Å, $\eta = 0.025$, and $a_s = 0.326$ Å. In fact, the relatively low value of Φ_0 as compared to other crystals allows one to neglect quantum effects also at relatively high electron energies. The depth $\Phi_M = \Phi(0)$ of the potential in diamond is such that $U_M = U(0) = -103$ eV, where $U(\rho) = e\Phi(\rho)$ is the electron potential energy (units with $\hbar = c = 1$ and $\alpha = e^2 \approx 1/137$ are employed throughout).

In general, the channeling regime of interaction features ultrastrong electromagnetic fields, which can lead to substantial energy loss of the radiating electron. In order for quantum effects to be negligible, we require that $\chi = \gamma_0 E/E_{cr} \ll 1$ [22], where γ_0 is the initial Lorentz factor of the electron, E is a measure of the amplitude of the electric field $\boldsymbol{E}(\boldsymbol{\rho}) = -\boldsymbol{\nabla}\Phi(\rho) = (2\Phi_0/a_s)\boldsymbol{\varrho}/[(\eta + \varrho^2 + (\eta + \varrho^2)^2]$ in the crystal, and $E_{cr} = m^2/|e| = 1.3 \times 10^{16}$ V/cm is the critical electric field of QED. By employing $E \sim \Phi_M/\rho_c$ as an estimate of E, it is $\chi = 1.5 \times 10^{-5}\varepsilon_0[\text{GeV}]|U_M[\text{eV}]|/\rho_c[\text{Å}]$.

In the classical regime $\chi \ll 1$ the electron dynamics including RR effects is described by the LL equation [5]. The LL equation for an electron with arbitrary momentum $\boldsymbol{p}(t) = m\gamma(t)\boldsymbol{\beta}(t)$, with $\gamma(t) = \varepsilon(t)/m = 1/\sqrt{1 - \boldsymbol{\beta}^2(t)}$ and $\boldsymbol{\beta}(t) = \dot{\boldsymbol{r}} = d\boldsymbol{r}/dt$, reads:

$$\begin{aligned}
\frac{d\boldsymbol{p}}{dt} = &e\boldsymbol{E} + \frac{2}{3}\frac{e^2}{m}\Big\{ e\gamma(\boldsymbol{\beta} \cdot \boldsymbol{\nabla})\boldsymbol{E} + \frac{e^2}{m}(\boldsymbol{\beta} \cdot \boldsymbol{E})\boldsymbol{E} \\
&- \frac{e^2}{m}\gamma^2[\boldsymbol{E}^2 - (\boldsymbol{\beta} \cdot \boldsymbol{E})^2]\boldsymbol{\beta} \Big\}.
\end{aligned} \quad (2)$$

Here the first two terms of the RR force originate from the Schott term in the LAD equation whereas the last "damping" one corresponds to the Liénard formula. Unlike the first "derivative" term, however, the second term of the RR force is strictly related to the damping one as only their sum ensures that the on-shell condition $\varepsilon(t) = \sqrt{m^2 + \boldsymbol{p}^2(t)}$ is preserved during the electron motion. Now, we assume that the crystal extends from $z = 0$ to $z = L$ and that at the initial time $t = 0$, the electron's position and velocity are $\boldsymbol{r}_0 = (x_0, 0, 0)$, with $0 < x_0 \leq \rho_c$, and $\boldsymbol{\beta}_0 = (0, 0, \beta_{z,0})$, respectively $(\varepsilon_0 = m\gamma_0 = m/\sqrt{1 - \beta_{z,0}^2})$. With these initial conditions, due to the symmetry of the potential $\Phi(\rho)$, it is $y(t) = 0$ and $E_y(\boldsymbol{\rho}) = 0$ along the electron trajectory. Thus, Eq.

(2) substantially simplifies and only the equation

$$\frac{d\beta_x}{dt} = -\left(\frac{F_x}{\varepsilon} + \frac{2}{3}\frac{e^2}{m^2}\frac{dF_x}{dx}\beta_x\right)(1-\beta_x^2), \qquad (3)$$

for $\beta_x(t)$ is needed below, with $F_x(x) = |e|E_x(x,0)$.

If one first neglects RR, the total energy $\mathcal{E} = \varepsilon(t) + U(|x(t)|)$ is a constant of motion. In the ultrarelativistic regime $\gamma_0 \gg 1$ of interest here and for typical crystal parameters it results $|\beta_x(t)| \ll 1$, such that $\varepsilon(t) \approx \varepsilon_0[1 + \beta_x^2(t)/2]$ (see, e.g., [20, 21, 22]). Indeed, energy conservation implies that $|\beta_x(t)| \leq \sqrt{2|U_M - U(x_0)|/\varepsilon_0} \ll 1$ (recall that $|U(\rho)| \sim 100$ eV [21, 22]). Finally, with the considered initial conditions, the quantity $\beta_x(t)$ is periodic in time, with period $T_0 = \sqrt{8\varepsilon_0}\int_0^{x_0} dx/\sqrt{|U(x) - U(x_0)|}$ and angular frequency $\omega_0 = 2\pi/T_0$ [21].

3. Results

The considerations above allow us to evaluate the effects of RR on the electron dynamics analytically. In fact, as it can be verified *a posteriori*, it is safe to assume that $|\beta_x(t)| \ll 1$ and that $\beta_z(t) \approx 1$ also including RR. Thus, by multiplying Eq. (2) by $p_x(t)$ and by neglecting corrections proportional to $\beta_x^2(t) \sim |U_M|/\varepsilon_0$, it is easy to prove that

$$\varepsilon(t) = \frac{\varepsilon_0}{1 + (2/3)\alpha(\gamma_0/m^3)\int_0^t dt' F_x^2(x(t'))}, \qquad (4)$$

where the integral is performed along the electron trajectory. In order to get an analytical insight on the motion of the electron, we assume here that $|x(t)| \ll a_s\sqrt{\eta}$, such that $F_x(x) \approx F_0 x/a_s\sqrt{\eta}$ and $dF_x(x)/dx \approx F_0/a_s\sqrt{\eta}$, where $F_0 = |e|E_0 = 2|U_0|/a_s\sqrt{\eta}$, with $U_0 = e\Phi_0$ ($U_0 = -29$ eV for diamond). Equation (3) with $1 - \beta_x^2(t) \approx 1$ and Eq. (4) show that the electron dynamics along the x direction is characterized by three time scales: one, $T_0 \approx 2\pi/\sqrt{F_0/\sqrt{\eta}\varepsilon_0 a_s}$, proper of the Lorentz dynamics and two additional,

$$\tau_s = \frac{6}{\alpha}\frac{\eta}{\gamma_0}\left(\frac{E_{cr}}{E_0}\right)^2\left(\frac{a_s}{x_0}\right)^2\lambda_C, \quad \tau_d = \frac{3}{\alpha}\sqrt{\eta}\frac{E_{cr}}{E_0}a_s \quad (5)$$

introduced by RR and corresponding to the term proportional to $F_x^2(x)$ in Eq. (4) and to the one proportional to $dF_x(x)/dx$ in Eq. (3), respectively ($\lambda_C = 1/m = 3.9 \times 10^{-3}$ Å is the Compton wavelength). Now, it is $T_0[\text{Å}] = 1.4 \times 10^5 a_s[\text{Å}]\sqrt{\eta\varepsilon_0[\text{GeV}]/|U_0[\text{eV}]|}$, $\tau_s[\text{Å}] = 7.0 \times 10^{12}\eta^2 a_s[\text{Å}]^4/(\varepsilon_0[\text{GeV}]U_0[\text{eV}]^2 x_0[\text{Å}]^2)$, and $\tau_d[\text{Å}] = 2.7 \times 10^{10}\eta a_s[\text{Å}]^2/U_0[\text{eV}]$, thus for a typical initial energy of $\varepsilon_0 = 10$ GeV and for $x_0 = 0.2 a_s\sqrt{\eta}$ in diamond, it results $\tau_d/\tau_s \approx 0.044$ and $T_0/\tau_d \approx 23 T_0/\tau_s = 1.7 \times 10^{-3}$. This suggests to solve Eq. (3) by employing the method of separation of time scales, which provides $x(t) \approx x_0 \exp(-t/\tau_d)\cos(\varphi(t))$, where $\varphi(t) = \int_0^t dt'\omega_0(t')$, with $\omega_0^2(t) = F_0/\varepsilon(t)a_s$, and

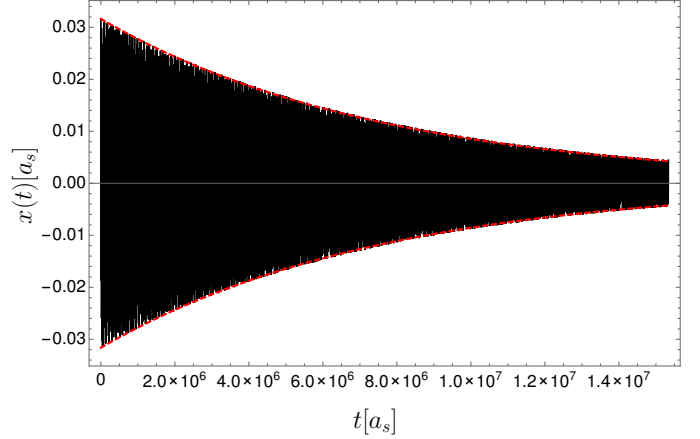$$\varepsilon(t) \approx \frac{\varepsilon_0}{1 + (\tau_d/\tau_s)[1 - \exp(-2t/\tau_d)]}. \qquad (6)$$

Figure 1: (Color online) The rapidly oscillating electron's coordinate $x(t)$ (continuous black curve) and the analytical expression $x_0\exp(-t/\tau_d)$ of the envelope (dashed red curve), for numerical parameters given in the text.
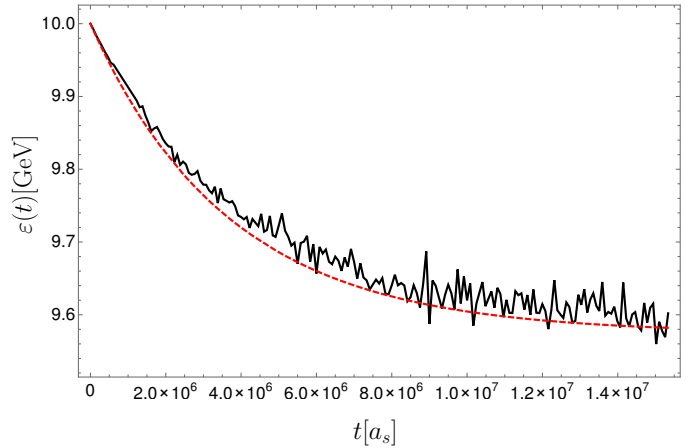

Figure 2: (Color online) Time evolution of the electron energy from a numerical integration of Eq. (2) (continuous black curve) and according to Eq. (6) (dashed red curve), for the same parameters as in Fig. 2.

In Fig. 1 and Fig. 2 we show a numerical example for diamond indicating the validity of the analytical estimation for $x(t)$ and for $\varepsilon(t)$ in Eq. (6) in comparison with a numerical integration of Eq. (2). The initial energy of the electron is 10 GeV, the initial position is $x_0 = 0.2 a_s\sqrt{\eta}$, and the final time corresponds to a crystal thickness of 0.5 mm (see also below). We have ensured numerically that the trend shown in the inset of Fig. 1, with RR "focusing" the electron's transverse motion to amplitudes much smaller than $a_s\sqrt{\eta}$, occurs for all allowed $x_0 \leq \rho_c$.

Now, RR effects are clearly larger for thicker crystals. However, an upper limit to "meaningful" values of the crystal thickness is set by the dechanneling, i.e., by the fact that, due especially to multiple Coulomb scattering, the transverse amplitude of the electron motion increases and, after a certain distance l_d (dechanneling length), the elec-
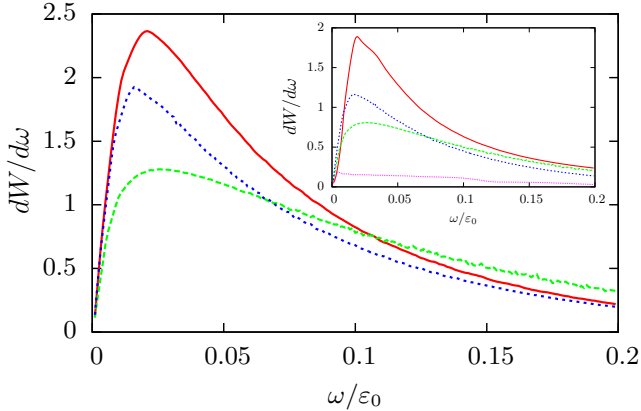
Figure 3: (Color online) Radiation energy spectra for parameters given in the text without RR (dashed green curve), with RR and no derivative term (dotted blue curve), and with RR (continuous red curve). The inset shows the corresponding plots including dechanneling and the spectrum of coherent bremsstrahlung by dechanneled electrons (fine-dotted purple line).

tron leaves the "channel" produced by the potential in Eq. (1) [21, 22]. The term "meaningful" above thus refers to the fact that for a crystal thickness larger than l_d, the electron will not anyway emit channeling radiation after a distance l_d. An order-of-magnitude estimate of the dechanneling length l_d for an electron initially propagating along the atomic string is given by $l_d = (\alpha/2\pi)(|U_M|\gamma_0/m)X_0$, where X_0 is the radiation length in the amorphous case ($X_0 = 12.2$ cm for diamond) [22]. In Fig. 3 three single-electron energy spectra $dW/d\omega$ are shown as a function of ω/ε_0, with ω being the emitted radiation angular frequency. The spectra are calculated by integrating the differential spectrum [1]

$$\frac{dW}{d\omega d\Omega} = \frac{e^2}{4\pi^2}\left|\int_{-\infty}^{\infty} dt \frac{\boldsymbol{n}\times[(\boldsymbol{n}-\boldsymbol{\beta})\times\dot{\boldsymbol{\beta}}]}{(1-\boldsymbol{n}\cdot\boldsymbol{\beta})^2}e^{i\omega(t-\boldsymbol{n}\cdot\boldsymbol{r})}\right|^2 \quad (7)$$

with respect to the solid angle Ω along the observation direction $\boldsymbol{n}$ (see also [25] for details) and by integrating numerically the exact LL equation (2) along the whole electron trajectory. In order to test specifically the importance of the derivative term in the LL equation (2), we show the spectrum without RR terms (dashed green curve), with RR terms except the derivative one (dotted blue curve), and with all RR terms (continuous red curve).

3.1. Discussion

The spectra in Fig. 3, obtained for diamond ($\boldsymbol{z} = \langle 111\rangle$), $\varepsilon_0 = 10$ GeV ($\chi = 0.02$[1]) and $L = l_d = 0.5$ mm, are averaged over a disk of radius ρ_c in the transverse plane

---

[1]Notice that, depending on the value of x_0, the maximum value E_M of the electric field experienced by the electron can be about $4E$, with the corresponding value $\chi_M = \gamma_0 E_M/E_{cr} \approx 0.08$ remaining still smaller than 0.1.

to simulate electrons impinging at different coordinates. Also, the free-electron laser parameter $K = \gamma_0\sqrt{2\langle\beta_x^2(t)\rangle}$, with $\langle f(t)\rangle = L^{-1}\int_0^L dt f(t)$, varies from 0 (for $x_0 = 0$) to 2.8 (for $x_0 = \rho_c$) without RR such that the local constant crossed field approximation [22], which requires $K \gg 1$, cannot be applied here. The main effect of RR is to increase the radiation yield at low frequencies thus shifting the position of the maximum of the spectrum to lower frequencies and the derivative term in the LL equation significantly enhances such effect. The shift of the maximum can be understood qualitatively as RR effects tend to reduce the electron energy and the average electric field experienced by the electron. The enhancement of RR effects due to the derivative term in the LL equation can be understood by noticing that the derivative dF_x/dx is largest at small x, where $dF_x/dx > 0$, such that since $e < 0$ the corresponding term in Eq. (2) acts as an additional "damping" term. The inset in Fig. 3 shows the corresponding spectra with dechanneling being included phenomenologically by dividing the crystal into $N = 50$ equal sections of length $\Delta L = L/N$ and by weighting the contribution of the jth section by means of the fraction of particles $\exp[-(j-1)\Delta L/l_d]$ remaining in the channel (see, e.g., [26]). The condition $\Delta L \ll L = l_d$ ensures that a small fraction of electrons dechannels on average in each section. One sees that the main effect of dechanneling, which resulted to be essentially insensitive to the exact value of N for large N's, is an overall reduction of the spectral yield, with no qualitative changes on the RR effects. Finally, we have ensured that the contribution of coherent bremsstrahlung from dechanneled electrons does not conceal RR effects (see the inset in Fig. 3). In order to include the latter effect, we have started from the differential cross section $d\sigma_{CB}(\omega, \theta, \varphi)/d\omega$ of coherent bremsstrahlung as presented, e.g., in Eq. (8.19) in [27] for the case at hand (an electron propagating at a small angle θ from the axis $\langle 111\rangle$ of diamond) and by averaging it with respect to the azimuthal angle φ of the initial electron momentum. In order to take into account that only dechanneled electrons emit coherent bremsstrahlung, we have assumed that the number of electrons in the channel as a function of the depth z is given by

$$N_e(z) = N_{e,0}e^{-z/l_d}, \quad (8)$$

where $N_{e,0}$ is the initial number of electrons. As an electron dechannels with a uniformly distributed value of φ, if we consider N sections of the crystal of length $\Delta L = L/N$, we can estimate the single particle energy spectrum per unit frequency due to coherent bremsstrahlung by the sum of contributions from each section given by $dW_j(\omega, \theta_j, \varphi)/d\omega = \rho_n\omega\Delta L d\sigma_{CB}(\omega, \theta_j, \varphi)/d\omega$, multiplied by the fraction $1 - \exp[-(j-1)\Delta L/l_d]$ of electrons in the
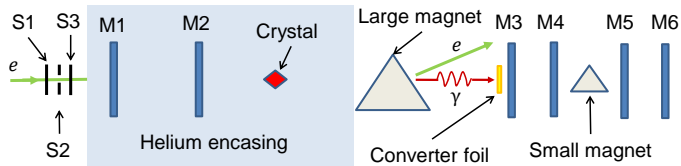
Figure 4: Sketch of a possible experimental setup (top view). S1-S3 denote scintillators and M1-M6 denote position-sensitive MIMOSA detectors [29].

section and averaged with respect to φ:

$$
\begin{aligned}
\frac{dW_{CB}}{d\omega} =& \rho_n \omega \Delta L \sum_{j=1}^{N} \left[1 - e^{-(j-1)\Delta L/l_d} \right] \\
& \times \int_0^{2\pi} \frac{d\varphi}{2\pi} \frac{d\sigma_{CB}(\omega, \theta_j, \varphi)}{d\omega}.
\end{aligned}
\tag{9}
$$

Here ρ_n is the number density of atoms in diamond ($\rho_n = 1.76 \times 10^{23}$ cm^{-3}). Now, a suitable value of the angle θ_j for each section j has still to be inserted in Eq. (9). Due to multiple Coulomb scattering, the nonprojected angle θ for electrons crossing an amorphous medium (the crystal acts essentially as an amorphous medium for above-barrier, dechanneled particles) is distributed according to a Gaussian distribution with standard deviation depending on z and given by (see, e.g., [28])

$$
\sigma_\theta(z) = \frac{13.6 \text{ MeV}}{\varepsilon_0} \sqrt{\frac{2z}{X_0}} \left(1 + 0.038 \ln \frac{z}{X_0} \right),
\tag{10}
$$

where X_0 is the radiation length ($X_0 = 12.2$ cm for diamond). In this way, we can estimate θ_j as the average value of θ of the particles over the solid angle $d\Omega = \sin\theta d\theta d\phi \approx \theta d\theta d\phi$, with $\theta \geq \theta_c$ where $\theta_c = \sqrt{2|U_M|/\varepsilon_0}$ is the Lindhard critical angle:

$$
\theta_j = \frac{\int_{\theta_c}^{\infty} d\theta\, \theta^2 e^{-\theta^2/2\sigma_{\theta,j}^2}}{\int_{\theta_c}^{\infty} d\theta\, \theta e^{-\theta^2/2\sigma_{\theta,j}^2}},
\tag{11}
$$

where $\sigma_{\theta,j} = \sigma_\theta((j-1)\Delta L)$.

By dividing the crystal into 50 sections, we have obtained the results shown as a fine-dotted purple line in the inset in Fig. 3.

3.2. Experimental considerations

Measurement of the spectra in Fig. 3 is possible using a setup as shown in Fig. 4. After passing the scintillators S1-S3, the electrons go through two position-sensitive MIMOSA detectors M1 and M2 [29] encased in Helium to reduce multiple scattering, in order to determine their incoming angle [30]. By deflecting the charged particles outgoing from the crystal via the large magnet, only the emitted photons hit a converter foil to produce electron-positron pairs. By measuring the energy of the pairs employing the small magnet, the energy of the photons can be

determined. The case considered here of electrons initially moving along the atomic string is a reasonable approximation as long as the electrons impinge with angles to the atomic string on a scale of order of or smaller than the Lindhard critical angle θ_c. Electrons with an angular divergence comparable to θ_c can indeed be achieved at the CERN SBA [31]. The spectra in Fig. 3 correspond to each electron emitting approximately 4.1 photons capable of pair production in the converter foil. In order to avoid pileup and obtain single-photon spectra, the converter foil should have correspondingly a thickness smaller than about one fourth of the radiation length. The peak of the red curve in the inset in Fig. 3 corresponds to a maximum of the number spectrum $dN_\gamma/d\omega = \omega^{-1}dW/d\omega$ of 1.1×10^{-8} eV^{-1} at 131 MeV and with a FWHM of 260 MeV. In order to resolve this maximum in 100 bins with 10^4 counts in each bin corresponding to an uncertainty of 1%, which would allow to discriminate among the three higher peaks of the curves in the inset in Fig. 3, would thus require about 1.4×10^7 electrons. At the CERN SBA a rate of 2000 electrons per minute can be achieved implying a measurement time of about five days.

4. Conclusions

In conclusion, we have demonstrated that the predictions of the LL equation can be feasibly tested experimentally by measuring the channeling radiation emitted by an ultra-relativistic electron beam impinging onto a diamond crystal slab. Most importantly, the effects of the derivative term in the LL equation are shown to affect in a measurable way the emission spectra. The required experimental conditions are available at the CERN SBA beamlines.

References

References

[1] J. D. Jackson, Classical Electrodynamics, Wiley, New York, 1975.
[2] M. Abraham, Theorie der Elektrizität, Teubner, Leipzig, 1905.
[3] H. A. Lorentz, The Theory of Electrons, Teubner, Leipzig, 1909.
[4] P. A. M. Dirac, Proc. R. Soc. London, Ser. A 167 (1938) 148.
[5] L. D. Landau, E. M. Lifshitz, The Classical Theory of Fields, Elsevier, Oxford, 1975.
[6] A. O. Barut, Electrodynamics and Classical Theory of Fields and Particles, Dover Publications, New York, 1980.
[7] F. V. Hartemann, High-Field Electrodynamics, CRC Press, Boca Raton, 2001.
[8] F. Rohrlich, Classical Charged Particles, World Scientific, Singapore, 2007.
[9] R. T. Hammond, Electron. J. Theor. Phys. 7 (2010) 221.
[10] A. Di Piazza, C. Müller, K. Z. Hatsagortsyan, C. H. Keitel, Rev. Mod. Phys. 84 (2012) 1177.
[11] D. A. Burton, A. Noble, Contemp. Phys. 55 (2014) 110.
[12] H. Spohn, Europhys. Lett. 50 (2000) 287.
[13] V. S. Krivitskii, V. N. Tsytovich, Sov. Phys. Usp. 34 (1991) 250.
[14] A. G. R. Thomas, C. P. Ridgers, S. S. Bulanov, B. J. Griffin, S. P. D. Mangles, Phys. Rev. X 2 (2012) 041004.
[15] A. Gonoskov, A. Bashinov, I. Gonoskov, C. Harvey, A. Ilderton, A. Kim, M. Marklund, G. Mourou, A. Sergeev, Phys. Rev. Lett. 113 (2014) 014801.

[16] N. Kumar, K. Z. Hatsagortsyan, C. H. Keitel, Phys. Rev. Lett. 111 (2013) 105001.

[17] M. Tamburini, C. H. Keitel, A. Di Piazza, Phys. Rev. E 89 (2014) 021201.

[18] A. Zhidkov, S. Masuda, S. S. Bulanov, J. Koga, T. Hosokai, R. Kodama, Phys. Rev. ST Accel. Beams 17 (2014) 054001.

[19] T. Heinzl, C. Harvey, A. Ilderton, M. Marklund, S. S. Bulanov, S. Rykovanov, C. B. Schroeder, E. Esarey, W. P. Leemans, Phys. Rev. E 91 (2015) 023207.

[20] X. Artru, M. Chevallier, Rad. Eff. Def. in Solids 130 (1994) 415.

[21] A. I. Akhiezer, N. F. Shul'ga, High-Energy Electrodynamics in Matter, Gordon and Breach Publishers, Amsterdam, 1996.

[22] V. N. Baier, V. M. Katkov, V. M. Strakhovenko, Electromagnetic Processes at High Energies in Oriented Single Crystals, World Scientific, Singapore, 1998.

[23] U. I. Uggerhøj, Rev. Mod. Phys. 77 (2005) 1131.

[24] H. Wiedemann, Synchrotron Radiation, Springer, Berlin, 2003.

[25] T. N. Wistisen, Phys. Rev. D 90 (2014) 125008.

[26] A. V. Korol, A. V. Solov'yov, W. Greiner, J. Phys. G: Nucl. Part. Phys. 27 (2001) 95.

[27] M. L. Ter-Mikaelian, High-Energy Electromagnetic Processes in Condensed Matter, Wiley-Interscience, Toronto, 1972.

[28] K. A. O. et al. (Particle Data Group), Chin. Phys. C 38 (2014) 090001.

[29] M. Winter, Nucl. Instr. Meth. A 623 (2010) 192.

[30] K. Kirsebom, U. Mikkelsen, E. Uggerhøj, K. Elsener, S. Ballestrero, P. Sona, S. Connell, J. Sellschop, Z. Vilakazi, Nucl. Instr. Meth. B 174 (2001) 274.

[31] Secondary Beams and Areas (SBA), http://sba.web.cern.ch/sba/ (2014).